https://doi.org/10.3311/PPci.37254

Periodica Polytechnica Civil Engineering

Numerical Simulation of GFRP-reinforced Rectangular Concrete Beams and Proposed Design Expressions

Gökhan Barış Sakcalı[1*], İsa Yüksel[1]

[1] Department of Civil Engineering, Faculty of Engineering and Natural Sciences, Bursa Technical University, Mimar Sinan Mahallesi, Mimar Sinan Bulvarı, Eflak Caddesi, Nos. 177, 16310 Yıldırım, Bursa, Türkiye
[*] Corresponding author, e-mail: gokhan.sakcali@btu.edu.tr

Received: 03 May 2024, Accepted: 23 October 2024, Published online: 18 November 2024

Abstract

Rebar corrosion, which has emerged as a primary detrimental factor, significantly impacts the structural performance, durability, and overall serviceability of reinforced concrete (RC) structures. In response to this issue, the growing use of GFRP, which offers superior corrosion resistance compared to steel, highlights the need to compare its performance with traditional steel-reinforced beams. To address this need, this study aims to evaluate the flexural behavior of beams reinforced solely with GFRP rebar and assess their structural performance relative to steel-reinforced beams. To achieve this, finite element models of both steel-reinforced and GFRP-reinforced beams were developed using ANSYS software. The analysis focused on load-bearing capacities, displacement characteristics, and crack patterns, and included the calculation of strain energies corresponding to collapse prevention performance limits. Overall, the study concludes that these modifications enhance design guidelines for GFRP-reinforced beams, offering improved practical applications in structural design. Significant findings include the proposed modification to the minimum reinforcement ratio equation in ACI 440.1R-15 for GFRP-reinforced concrete, the introduction of a suggested strain reduction factor for GFRP rebar, and the revision of the effective moment of inertia equation with coefficients of 0.05 and 0.95. These revisions improved the general performance indicator to 1.17, yielding better results compared to other equations in the literature. The study concludes that these modifications enhance design guidelines for GFRP-reinforced beams, offering improved practical applications in structural design.

Keywords

beam, crack propagation, FEM, flexure, GFRP rebar, steel rebar

1 Introduction

Rebar corrosion, which has emerged as the primary detrimental factor, significantly impacts the structural performance, durability, and overall serviceability of reinforced concrete (RC) structures. The detrimental effects of rebar corrosion manifest in three primary ways. First, rebar corrosion initiates concrete damage, manifesting as cracks and eventually leading to spalling of the concrete cover. This initial consequence not only compromises the structural integrity but also poses a threat to the overall durability of RC structures. Second, the corrosion process induces a reduction in the cross-sectional area of the rebar. This, in turn, adversely affects the steel stress and strains, contributing to further deterioration of the structural performance. The third significant consequence of rebar corrosion lies in the diminished bond strength at the interface between the rebar and the concrete. This decrease in bond strength exacerbates structural vulnerabilities, creating additional challenges for the overall serviceability of RC structures [1–3]. To mitigate the adverse impacts mentioned above, the concept of manufacturing rebar from a noncorrosive material is highly desirable. Presently, fiber-reinforced polymer (FRP) rebars are being applied extensively, particularly as longitudinal reinforcements in various infrastructure projects. In addition to preventing the decrease in bearing capacity caused by corrosion, FRP reinforcing bars offer several advantages over conventional steel rebars. In addition to their exceptional corrosion resistance, these rebars boast a lightweight nature and nonconductive properties. With a significantly higher tensile strength than traditional rebar, FRP reinforcement is particularly well suited for longitudinal applications [4–8]. While steel rebars can induce electromagnetic interference, FRP composites exhibit transparency to radio waves and electromagnetic

Cite this article as: Sakcalı, G. B., Yüksel, İ. "Numerical Simulation of GFRP-reinforced Rectangular Concrete Beams and Proposed Design Expressions", Periodica Polytechnica Civil Engineering, 2024. https://doi.org/10.3311/PPci.37254

interference transmissions. Nevertheless, it is essential to acknowledge that the mechanical behaviors of FRPs and steel rebars differ significantly. Various design recommendations or guidelines, such as ACI 440.1R-06 [9], ACI 440.1R-15 [10], CSA S6-14 [11], and CSA S806-12 (R2021) [12], have been developed to assist in the design of RC elements with FRP rebars. Despite these positive attributes, FRP rebars present challenges in bending at construction sites, requiring prebending and preparation during factory production. Moreover, the strength decreases when FRP rebars undergo bending. Using FRP reinforcing bars as stirrups in RC elements becomes challenging due to this factor. For this reason, these FRP rebars can be utilized in conjunction with traditional steel rebars, creating a hybrid reinforcement system. To mitigate the capacity reduction in RC elements caused by corrosion, the use of FRP rebars exclusively in RC elements has garnered increased amounts of attention. However, the mechanical behavior of FRP rebar differs significantly from that of steel rebar, necessitating further research. Unlike steel, which exhibits a bilinear response under uniaxial tensional force, FRP rebar exhibit linear behavior until rupture. The brittle nature of FRP rebar dominates the failure mode, transforming the behavior of a concrete element equipped with FRP rebar into an overall brittle characteristic. Moreover, FRP rebars encounter challenges when subjected to compressive stress, as they do not exhibit the same behavior as steel. The type of fiber used plays a crucial role in determining the properties of FRP rebar, with each fiber type presenting distinct advantages and disadvantages. Glass fiber reinforced polymer (GFRP) rebars, which employ glass fibers, have emerged as the most widely used type of FRP rebar. This popularity is attributed to the notable advantages of these materials, including low cost, high tensile strength, and resistance to high temperatures and chemicals.

Numerous studies have explored the impact of GFRP rebar on the bending behavior of RC elements in recent years [13–17]. In these studies, many parameters, such as the differences between FRPs and steel reinforcing bars, behavioral differences when used as reinforcements in beams, deformation properties, ductility and failure modes, and crack propagation conditions, were studied. It has been observed that as the concrete strength and reinforcement ratio increase in RC elements reinforced with GFRP, the load-carrying capacity also improves. However, a higher reinforcement ratio may lead to a reduction in the ultimate displacement of these elements.

The Young's Modulus of GFRP rebars is generally lower than that of steel rebars. Consequently, in comparison to conventional RC members, the deformation and crack width become more significant for GFRP-reinforced structures. The effective moment of inertia also changes due to the low Young's Modulus, necessitating modifications to the design equations typically used for steel-reinforced elements. Despite the brittle nature of GFRP rebar, which contributes to a more brittle behavior in the RC elements in which it is used, its high tensile strength and resistance to corrosion present it as a viable alternative to steel reinforcement. However, there is a consensus that more experimental and analytical studies are needed to deepen the understanding of the bending behavior of GFRP-reinforced RC elements. Additionally, new strength reduction factors may need to be developed to support innovative design approaches [17]. Furthermore, factors such as energy dissipation and failure mode should be taken into account when designing concrete members with FRP rebar, given the linear stress-strain relationship characteristic of this material [18].

The bending stiffness of the RC beam, which cracks due to bending, decreases. These stiffness reductions that may occur in RC beams due to cracking are eliminated by considering the stiffness of the cracked section in the flexural stiffness calculation. Since the Young's modulus of FRP rebar is generally lower than the Young's modulus of steel rebar, the cracked section stiffness may be different in FRP-reinforced sections. This situation directly affects the RC element and system displacements. For this reason, the development of new computational approaches has come to the fore in determining the effective moments of inertia of RC elements with FRP rebars. The cracked section stiffness of RC beams with FRP rebar depends on the correct determination of the effective moments of inertia. In determining the effective moment of inertia, ACI 440.1R-06 [9]; ACI 440.1R-15 [10]; Bischoff [19, 22]; Rafi and Nadjai [20]; ISIS [21] and Habeeb and Ashour [23] suggested using Eqs. (1)–(7), respectively:

$$I_e = \frac{I_{cr}}{1-\eta\left(\frac{M_{cr}}{M_a}\right)^2} \quad \text{where } \eta = 1-\frac{I_{cr}}{I_g} \tag{1}$$

$$I_e = \beta_d\left(\frac{M_{cr}}{M_a}\right)^3 I_g + \left[1-\left(\frac{M_{cr}}{M_a}\right)^3\right] I_{cr} \le I_g \quad \text{where } \beta_d = \frac{1}{5}\left(\frac{\rho_f}{\rho_{fb}}\right) \le 1 \tag{2}$$

$$I_e = \beta_d \left(\frac{M_{cr}}{M_a}\right)^3 I_g + \left[1 - \left(\frac{M_{cr}}{M_a}\right)^3\right] \frac{I_{cr}}{\gamma} \le I_g \quad \text{where } \beta_d = \frac{1}{5}\left(\frac{\rho_f}{\rho_{fb}}\right) \le 1 \tag{3}$$

$$I_e = \frac{I_g I_{cr}}{I_{cr} + \left(1 - 0.5\left(\frac{M_{cr}}{M_a}\right)^2\right) \times \left(I_g - I_{cr}\right)} \tag{4}$$

$$I_e = \left[1 + 2.3 \times \left(\frac{M_{cr}}{M_a}\right)^3 \times I_{cr}\right] \tag{5}$$

$$I_e = \beta_d \left(\frac{M_{cr}}{M_a}\right)^3 I_g + \gamma_G \left[1 - \left(\frac{M_{cr}}{M_a}\right)^3\right] I_{cr} \le I_g \quad \text{where } \beta_d = \frac{1}{5}\left(\frac{\rho_f}{\rho_{fb}}\right) \le 1;\ \gamma_G = 0.6 \tag{6}$$

$$I_e = \frac{I_{cr}}{1 - \gamma\left(\frac{M_{cr}}{M_a}\right)^2 \left[1 - \frac{I_{cr}}{I_g}\right]} \quad \text{where } \gamma = 1.72 - 0.72\left(\frac{M_{cr}}{M_a}\right), \tag{7}$$

where I_e is the effective moment of inertia, M_a is the maximum moment in the member at stage deflection, M_{cr} is the cracking moment, I_{cr} is the moment of inertia of the transformed cracked section, I_g is the gross moment of inertia, ρ_f is the ratio of FRP reinforcement, ρ_{fb} is the ratio of FRP balanced reinforcement, β_d is the first-term reduction coefficient for RC elements with FRP rebars, γ is a factor, η is the coefficient depending on I_{cr} and I_g, and γ_G is the second-term reduction coefficient for RC elements with FRP rebars.

By using an accurate numerical modeling technique, the structural behavior and failure modes of RC elements can be determined without the need for a laboratory environment [4]. Studies on finite element modeling (FEM) of FRP-reinforced elements have gained momentum in recent years [4, 8, 24–26]. As a result of these developments, structural behavior can be reflected quite realistically using the FEM. Although the current use of FEMs requires much research, the creation of FEMs is highly important for parametric studies. The behavior of FRP-reinforced elements in the FEM depends on the correct definition of the concrete yield criteria [4, 8].

The aim of this study is to propose a reduction factor for GFRP rebar and revised equations for the design of GFRP-reinforced concrete elements, based on strain energy. This approach not only aims to improve the accuracy of current design models but also provides a deeper understanding of the element behavior. The findings of this study have the potential to significantly reshape the design equations currently used for FRP-reinforced concrete elements, offering novel insights and contributing a fresh perspective to the design process. This study presents the findings of a finite element numerical case study, focusing on the behavioral distinctions observed in GFRP-reinforced beams. This investigation specifically compares beams reinforced with GFRP bars for tensile reinforcement against beams employing conventional steel reinforcement, with a particular emphasis on strain energy. To achieve this goal, beam models with identical geometric properties but different reinforcement types and ratios were developed. Through the application of the FEM, these models recognized comprehensive analysis. The results were then scrutinized in conjunction with established relationships found in the literature. This study provides insightful suggestions that could prove valuable in the design of GFRP-reinforced beams. By elucidating the nuanced behavioral differences between GFRPs and conventional steel reinforcements, this research contributes to advancing our understanding and informing more effective design practices.

2 Material properties of the GFRP rebar

FRP rebar do not exhibit yielding behavior prior to failure. Instead, they behave linearly elastically until they fail under tensile forces. This distinctive characteristic sets FRP rebars apart from traditional steel counterparts, impacting their structural performance. While the ultimate tensile strength of FRP rebars typically surpasses that of steel rebars, it is important to note that their Young's modulus and ultimate strain values are generally lower. This divergence in material properties highlights the need for a nuanced approach when designing structures that incorporate FRP rebars.

The tensile strength of FRP rebars exhibits high variability, primarily dependent on factors such as the matrix material, the type of fiber used, and the ultimate strength of the fiber itself. For this reason, it is very important to experimentally determine the tensile strength and Young's modulus of the FRP reinforcing bars used in these studies. Prior to this study, the authors conducted laboratory tests on five

GFRP rebar samples obtained from local manufacturers following the ASTM D7205/D7205M-06(2011) [27] standard. The mechanical properties obtained from these tests were described previously [7]. The average tensile strength and Young's modulus of the GFRP rebar were determined to be 799 MPa and 41,341 MPa, respectively [7]. The tensile strength of the GFRP rebar varies in the range of 483–1600 MPa, while Young's modulus varies in the range of 35–50 GPa according to ACI PRC-440-07 [28]. These test results for the GFRP rebar used in the numerical models comply with the ACI PRC-440-07 [28] standard.

3 3D finite element model

ANSYS software [29] is used for modeling the beams via the finite element method. To model the concrete element by this software, the element type Solid 65, which is suitable for modeling three-dimensional solid elements considering nonlinear behavior with or without rebar, was used [1, 30]. The cracking and crushing properties of concrete were also considered by this element type, with eight nodes that can be displaced in three directions [29]. The concrete compressive material model was developed based on Eqs. (8)–(10) [31] (Fig. 1 (a)). In this formulation, the initial point on the stress–strain curve is set at 30% of the ultimate compressive strength, taking into account Hooke's law and Young's modulus [32]. Equation (11) was employed for the calculation of Young's modulus (E_c) [33]. In addition, Eq. (12), derived from the tensile bending strength of concrete, was used to calculate the tensile strength of concrete (f_{ct}) [34]:

$$f = \frac{E_c \varepsilon}{1 + \left(\frac{\varepsilon}{\varepsilon_0}\right)^2} \text{ for nonlinear region} \tag{8}$$

$$f = E_c \varepsilon \text{ for linear region} \tag{9}$$

$$\varepsilon_0 = \frac{2 f_c}{E_c} \tag{10}$$

$$E_c = 5000\sqrt{f_c} \tag{11}$$

$$f_{ct} = 0.64\sqrt{f_c} \tag{12}$$

where ε is the strain, ε_0 is the strain corresponding to the maximum stress of unconfined concrete, and f is the stress corresponding to each strain.

Realistically performing nonlinear analyses requires accurate definitions of the material's yield criteria. These criteria differ based on the material's ductile or brittle behavior, underscoring the crucial importance of precise characterization. The Willam–Warnke yield criterion [35] was preferred for the modeling of concrete, which is a quasi-brittle material. This criterion can take into account crushing and cracking of concrete and can also be used for concrete subjected to multiaxial stress. The determination of the yield surface involves utilizing principal stresses and five distinct parameters. Elements surpassing this yield surface may experience either cracking due to tensile stresses or crushing due to compressive

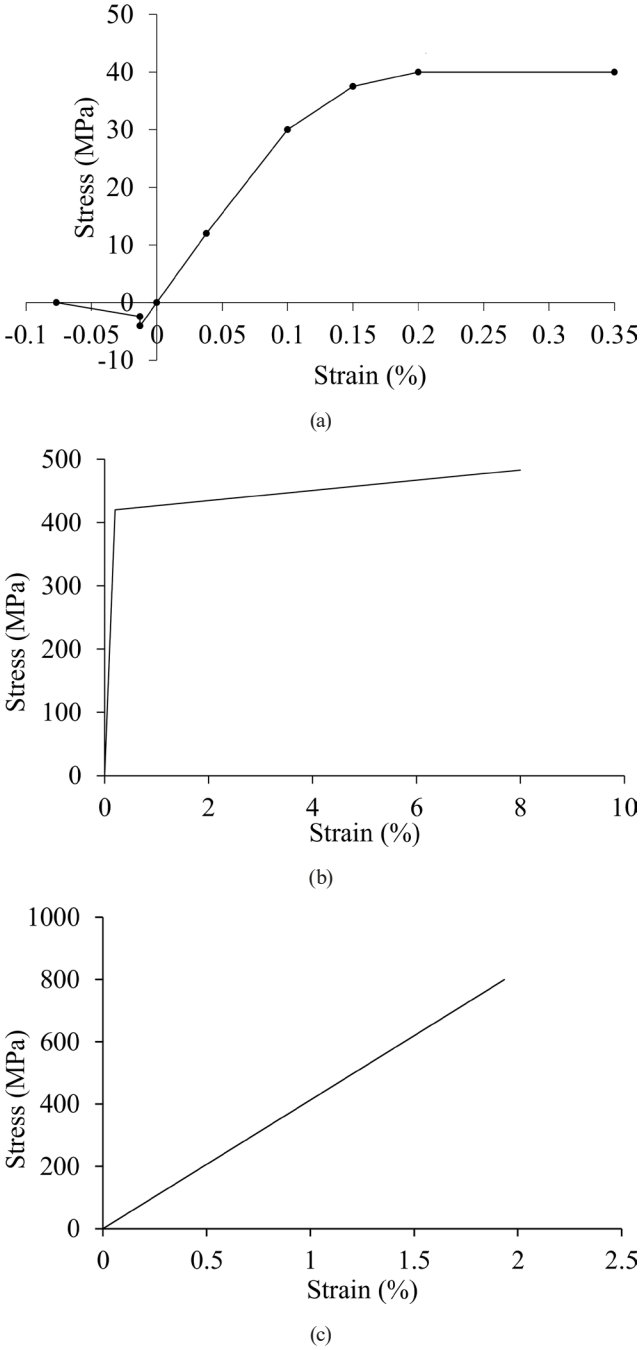

Fig. 1 Stress–strain relationships of the materials: (a) concrete, (b) steel rebar, and (c) GFRP rebar

stresses. To accurately define the yield surface, it is essential to establish shear transfer coefficients for both open and closed cracks. The shear stress transfer coefficients used in this study were selected as 0.2 and 0.8, respectively, considering the references [32, 36, 37].

A bilinear isotropic behavior model was also proposed in the new Turkish earthquake code, BECT-2018 [33], for steel rebar considering strain hardening. This model can be defined by yield and tensile strength and strains corresponding to these strength values. These parameters were selected as 420 MPa and 483 MPa, and their corresponding strains were 0.002 and 0.08, respectively (Fig. 1 (b)). Furthermore, it was assumed that the material behavior of the GFRP rebar was linear elastic, as depicted in Fig. 1 (c). The Poisson's ratio for steel was considered to be 0.3, while for the GFRP rebar, it was taken as 0.2.

The bond-slip relationship between the steel reinforcing bar and the concrete interface was determined utilizing Eqs. (13)–(17) [38], as illustrated in Fig. 2 (a). To incorporate the bond-slip relationship in RC elements with spiral-surfaced GFRP rebars, adjustments were implemented by referencing Vint's work [39], specifically modifying Eqs. (13), (18), (19), as illustrated in Fig. 2 (b). To comprehensively capture the interaction between the concrete and rebar in terms of bond-slip, nonlinear spring elements were introduced. To comprehensively model the interaction between the concrete and rebar concerning bond slip, two joints were combined using the Combin39 element type, recognized for its nonlinear spring characteristics. This approach takes into account the force–displacement relationship, providing a more accurate representation of the structural behavior in relation to the bond–slip characteristics [29].

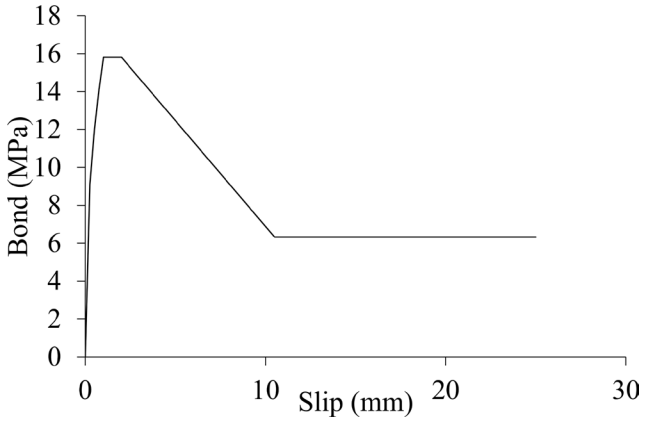

(a)

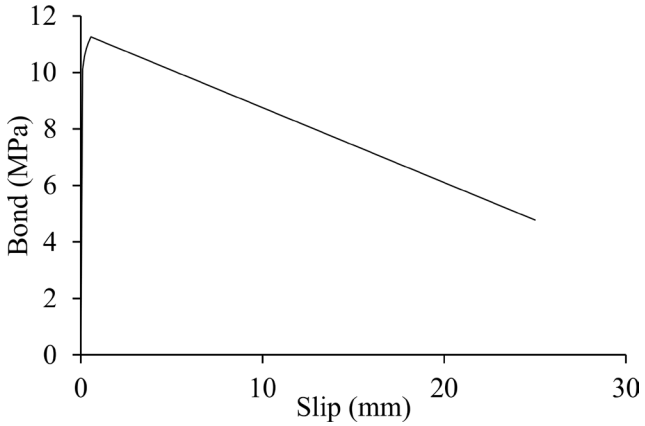

(b)

Fig. 2 Bond-slip relationships of the (a) steel rebar and concrete interface and (b) GFRP rebar and concrete interface

$$\tau_{\max} = 2.5\sqrt{f_c} \tag{13}$$

$$\tau = \tau_{\max}\left(\frac{s}{s_1}\right)^{0.4} \quad 0 \le s \le s_1 \tag{14}$$

$$\tau = \tau_{\max} \quad s_1 \le s \le s_2 \tag{15}$$

$$\tau = \tau_{\max} - \left(\tau_{\max} - \tau_f\right)\left(\frac{s - s_2}{s_3 - s_2}\right) \quad s_2 \le s \le s_3 \tag{16}$$

$$\tau = \tau_{bf} \quad s_3 \le s \tag{17}$$

$$\tau = \tau_{\max}\left(\frac{s}{s_{\max}}\right)^{0.0622} \quad 0 \le s \le s_{\max} \tag{18}$$

$$\tau = \tau_{\max}\left(1 - 0.0131\left(\frac{s}{s_{\max}} - 1\right)\right) \quad s_{\max} < s \tag{19}$$

Where $\tau_{\max}$ is the maximum shear stress, τ is the bond strength, s is the slip and f_c is the compressive strength of the concrete. The $s_{\max}$ is the slippage corresponding to the maximum shear stress. Additionally, s_1 is the slip corresponding to the starting point of the maximum bond stress, s_2 is the slip corresponding to the end point of the maximum bond, s_3 is the slip corresponding to the starting point of the reduced bond stress, and τ_{bf} is the reduced bond stress. In this study, considering [38, 39], the following parameters were selected: $s_{\max} = 0.556$ mm, $s_1 = 1$ mm, $s_2 = 2$ mm, $s_3 = 10.5$ mm, and $\tau_{bf} = 0.4\tau_{\max}$.

Three different approaches (discrete model, embedded model, smeared model) are generally used in the modeling of RC composite elements composed of combined concrete and rebar [40–42]. These approaches involve replacing the concrete element group and reinforcement element group to ensure the continuity of the composite [43].

In this study, RC composite elements were modeled using the discrete model technique. This modeling technique is chosen to more accurately express the bond-slip relationship between the concrete and the rebar and to obtain economical solutions by shortening the analysis time.

The beam models created in this study are validated by using three test models available in the literature: Sample C216-D1 tested by Barris et al. [44] (Fig. 3 (a)), Sample GGu-10d/3p tested by El-Mogy et al. [37] (Fig. 3 (b)), and Sample 3-10 L tested by Ovitigala et al. [45] (Fig. 3 (c)). The load displacement relationships of the numerical models created in this study and the load displacement relationships of the experimental data were compared (Fig. 3). Apart from minor differences, as shown in Fig. 3, the numerical and experimental results seem to be quite compatible with each other.

The general view and cross-section of the created beam models are shown in Fig. 4. The samples were divided into five different element sizes (100 mm, 50 mm, 25 mm, 20 mm, and 10 mm), and a convergence study was carried out (Fig. 5). The displacement in the beam element divided into 25 mm meshes is approximately 0.5% greater than the displacement in the beam element divided into 10 mm meshes. Therefore, a mesh spacing of 25 mm was selected because the analysis was completed with an error of 0.5%.

In the analysis of beams with the 3D finite element method, the analysis time and number of elements can be reduced by utilizing symmetry. While defining the element or system divided by the symmetry axis, the boundary conditions must be defined so that the system continuity is maintained. A numerical model of the 3D beam depicted in Fig. 6 was established to evaluate the precision of the boundary conditions defined along the symmetry axes. A numerical model of the beam depicted in Fig. 6 was developed to assess the accuracy of the boundary conditions specified along the symmetry axes. As shown in Fig. 6, the beam is modeled as full, half and quarter. To benefit from symmetry in the analysis, the beam was first modeled as full, half and quarter, as shown in Fig. 6. The ultimate load bearing capacity and the vertical displacement capacity in the middle of the quarter span model were 0.6% lower and 1.9% greater, respectively, than those of the full model. As a result, the quarter model was used in the present study because there were negligible differences.

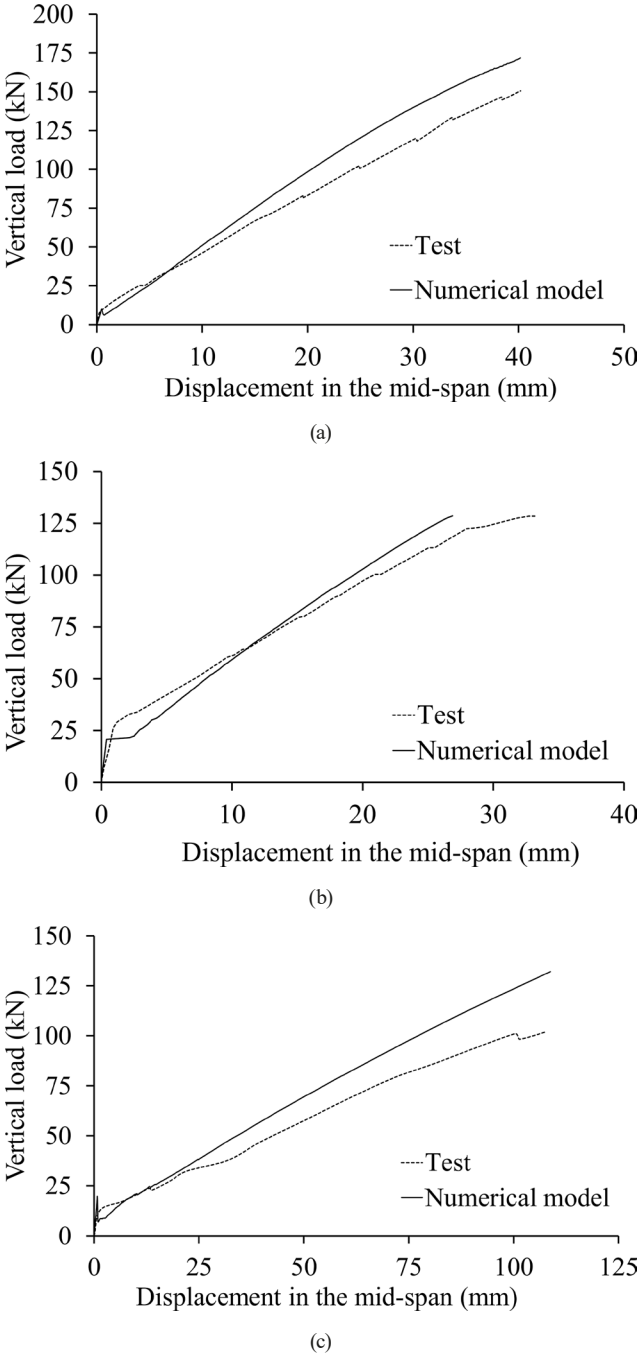

Fig. 3 Comparison of experimental data and numerical models for (a) Sample C216-D1 tested by Barris et al. [44], (b) Sample GGu-10d/3p tested by El-Mogy et al. [37], and (c) Sample 3-10 L tested by Ovitigala et al. [45]

4 Energy concept and numerical universality

The strain energy per unit volume, also known as the strain energy density, is a term used to describe the amount of energy stored within a material when subjected to deformation. Determination of this density involves calculating the area under the stress–strain curve up to the point of ultimate strain. Additionally, it serves as a crucial indicator of the material's ability to absorb and store mechanical energy before it reaches its breaking point. The trapezoidal rule, which is a numerical method, was used to calculate the strain energies of beam elements. According to

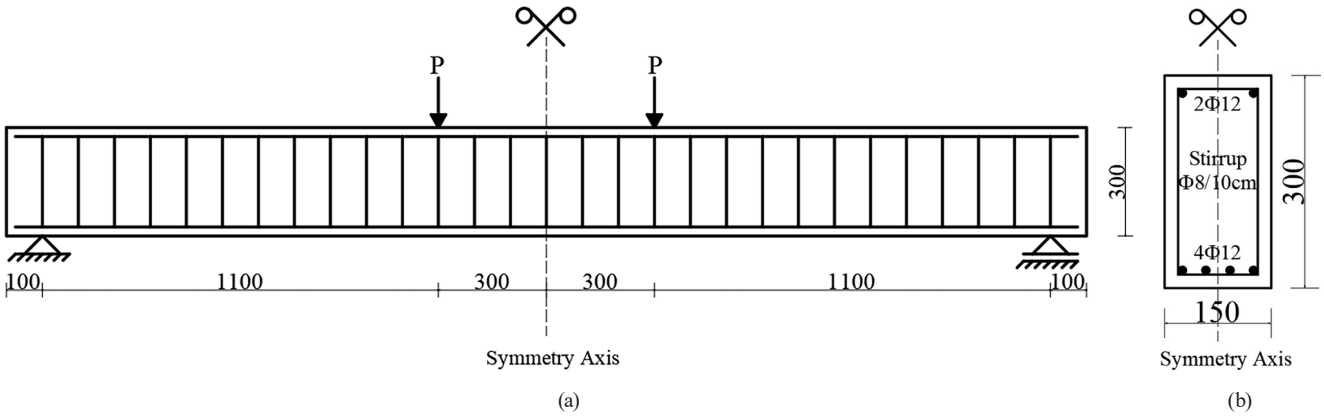

Fig. 4 Beam cross sections for the convergence study; (a) longitudinal cross section and (b) cross section

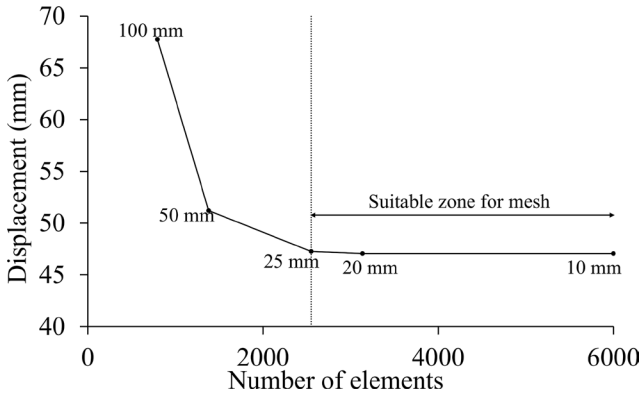

Fig. 5 Convergence study

strength-based design principles for beam section design, the moment capacity (M_r) of a section should be greater than or equal to the design moment (M_d). The assumption was made that the design moment equals the section moment capacity to elucidate the variances in behavior between steel and FRP-reinforced beams, as illustrated in Fig. 7. In addition, the tensile cracks that formed in the concrete were neglected, and it was assumed that the steel-reinforced beam behaved bilinear without strain hardening, as shown in Fig. 7. In Fig. 7, $\phi_{u,\mathrm{FRP}}$ and $\phi_{u,\mathrm{steel}}$ represent the ultimate curvatures corresponding to the FRP and steel rebar, respectively. Although both the steel- and FRP-reinforced concrete sections with the same moment capacity fulfill the design requirements, the steel-reinforced section has much greater strain energy than the FRP-reinforced section (Fig. 7). This has also been emphasized by Zhu et al. [24]. This situation reveals the necessity of designing RC beams with FRP rebars on the basis of strain energy. For this reason, in this study, we propose design suggestions for GFRP-reinforced sections based on the strain energy.

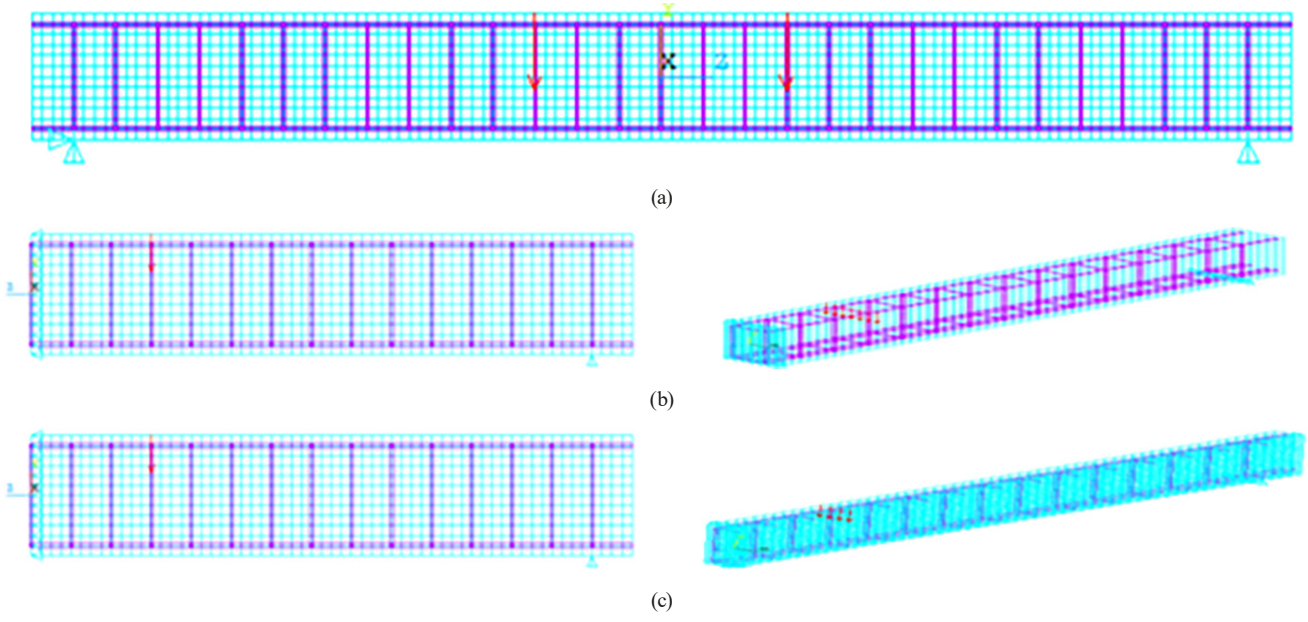

Fig. 6 Finite element models: (a) full model, (b) half model, and (c) quarter model

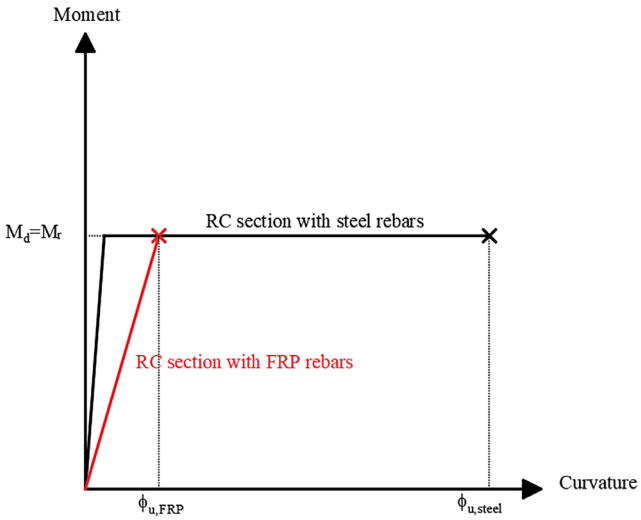

Fig. 7 Moment-curvature relationships of steel and FRP-reinforced beams for the design moment

For the beam model depicted in Fig. 8, the dimensions and reinforcement details are outlined in Table 1 for steel reinforcement and Table 2 for GFRP reinforcement. This detailed presentation facilitates an in-depth examination of the structural properties associated with each type of reinforcement. By offering a comprehensive overview, this paper lays the groundwork for a thorough analysis and comparison of the two scenarios. The minimum and maximum reinforcement ratios for the RC beams with steel rebar were determined to be 0.0042 and 0.02, respectively, according to TS 500 [46]. In contrast, for beams reinforced with GFRP rebar, the corresponding ratios were derived from ACI 440.1R-15 [10] and were found to be 0.0032 and 0.075. Significantly, the compressive strength of FRP rebar is notably lower than its tensile strength [3]. Consequently, in all the models featuring GFRP rebar, the compression rebar was assumed to be 2ϕ8, as it is anticipated that altering the compression rebar would not impact the models. Additionally, the concrete cover thickness and stirrup dimensions were uniformly set at 25 mm and ϕ8/100/200 mm, respectively, across all the models.

5 Results and discussion

5.1 Maximum load, displacement, and strain energy

When Table 2 is organized from smallest to largest based on the difference in tension and compression reinforcement ratios, it is observed that after approximately a 0.5% difference, the failure mode shifts from tension failure due to GFRP rupture to compression failure caused by the crushing of concrete under compression. This result highlights the significant limit at approximately 0.50% (ρ-ρ') that triggers the change in failure mode. Performing the same ranking solely based on the tension reinforcement ratio yields a similar limit value of approximately 0.60% (ρ). Considering that GFRP rebar acts as a compression reinforcement incapable of withstanding compressive forces, the ranking based on the tensile reinforcement ratio alone holds more significance. Assuming the ultimate strain of the concrete is ε_{cu} = 0.003, the balanced reinforcement ratio is calculated to be 0.572%. Table 2 reveals that the beams reached failure through either the rupture of GFRP rebar or the crushing of concrete; notably, both of these failure modes lacked ductility. In instances where the reinforcement ratio in the section was under-reinforced, the beam reached the collapse state due to the rupture of the GFRP rebar. In contrast, in cases where a higher reinforcement ratio is desired, the collapse of the beam occurs as a result of the crushing of the concrete in the compression zone. These findings align with the results obtained by Adam et al. [14]. As a result, similar to that of steel-reinforced beams, the balanced reinforcement ratio emerges as a crucial parameter determining the failure mode of RC with GFRP rebar. Nevertheless, it is important to note that both failure modes of these beams exhibit brittleness. In addition, the strain energy increases as the reinforcement ratio increases (for the same cross-sectional dimensions) in these beams up to the balanced reinforcement ratio. However, beyond this limit, the trend of strain energy increase stabilizes and remains relatively constant as the damage mode shifts

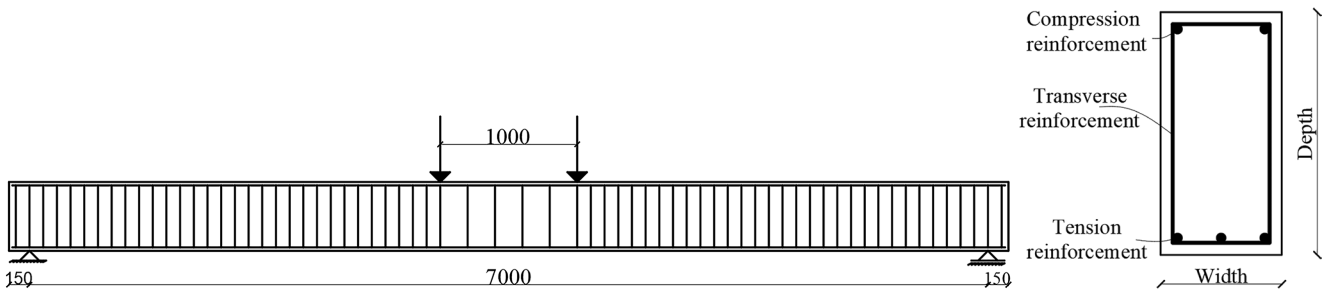

Fig. 8 RC beam with steel and GFRP rebar: (a) longitudinal cross section and (b) cross section

Table 1 Properties of steel-reinforced beams

Model code	Width (mm)	Depth (mm)	Tensile reinf. (ρ)	Comp. reinf. (ρ')	ρ-ρ'	Max. displ. (mm)	Max. load (kN)	The strain energy (kNm)
S1	250	500	3ϕ16	2ϕ14	0.00249	167.05	77.15	11.63
S2	250	500	3ϕ16	2ϕ16	0.00169	250.83	78.68	12.53
S3	250	500	3ϕ20	2ϕ14	0.00534	154.25	119.46	11.12
S4	250	500	3ϕ20	2ϕ18	0.00365	231.65	118.80	16.96
S5	250	500	3ϕ20	2ϕ20	0.00265	276.87	120.69	16.32
S6	250	500	4ϕ16	3ϕ14	0.00289	200.83	104.28	10.67
S7	250	500	4ϕ16	2ϕ16	0.00339	167.27	102.30	11.24
S8	250	500	5ϕ20	2ϕ20	0.00794	155.38	196.34	19.99
S9	250	600	3ϕ16	2ϕ12	0.00262	267.38	123.00	14.05
S10	250	600	3ϕ16	2ϕ14	0.00206	278.36	124.80	13.08
S11	250	600	3ϕ20	2ϕ16	0.00376	388.96	200.08	25.13
S12	250	600	3ϕ20	2ϕ20	0.00219	470.37	204.69	27.79
S13	250	600	4ϕ20	2ϕ22	0.00345	274.33	250.23	25.55
S14	250	600	5ϕ16	2ϕ14	0.00485	208.47	195.00	19.72
S15	250	600	5ϕ16	2ϕ18	0.00345	299.76	199.12	19.59
S16	300	600	4ϕ16	2ϕ14	0.00233	231.51	136.15	10.35
S17	300	600	4ϕ16	2ϕ14	0.00288	259.13	137.38	10.94
S18	300	600	4ϕ20	2ϕ16	0.00495	111.40	193.37	17.10
S19	300	600	4ϕ20	2ϕ20	0.00364	209.77	206.75	21.73
S20	300	600	4ϕ20	3ϕ20	0.00182	296.41	215.04	22.49
S21	300	600	5ϕ20	2ϕ18	0.00615	128.77	244.74	26.80
S22	300	600	5ϕ20	2ϕ22	0.00470	152.59	244.74	32.71
S23	300	600	5ϕ20	3ϕ20	0.00364	153.87	247.93	31.97
S24	300	600	5ϕ16	2ϕ14	0.00732	258.93	177.51	27.05
S25	300	600	5ϕ16	2ϕ18	0.00615	284.09	177.51	30.42

toward the fracture of the concrete (Table 2). This indicates that more strain energy can be absorbed by designing these beams, which are brittle in both failure modes, to reach the final state by crushing the concrete.

The G2 and G3 models, distinguished solely by their tensile reinforcement ratios, were subjected to a specific comparative analysis. In the G2 model, the tension reinforcement ratio remained below the balanced reinforcement ratio, registering at 0.508%. Conversely, in the G3 model, assuming ε_{cu} = 0.003, the ratio surpassed the balanced reinforcement level, reaching 0.643%, denoting a 27% increase. Notably, the G3 model exhibited higher values of maximum displacement, load-bearing capacity, and strain energy by 13.2%, 33.3%, and 53.5%, respectively, than did the G2 model. This striking observation lies in the substantial increase in the strain energy. In their study, Ifrahim et al. [47] reported that an increase in the reinforcement ratio from 0.62% to 1.76% resulted in a 58% increase in load capacity. In our study, a similar trend is observed, where an increase in the reinforcement ratio from 0.643% (G3 specimen) to 1.524% (G14 specimen) leads to an approximately 42% increase in the load capacity. This discovery is consistent with the findings presented by Ifrahim et al. [47] in their experimental and numerical investigations. However, it is paramount to highlight that while an increase in load capacity is often expected, it does not always correlate with an increase in strain energy, as evidenced by the G3 and G14 samples. This discrepancy arises from the reinforcement ratio's effect on enhancing the element's stiffness while concurrently diminishing its displacement capacity.

A further comparison between the G2 and G5 models, which have the same cross-sectional geometry but feature a nearly twofold increase in the tensile reinforcement ratio (classified as over-reinforced), revealed an increase in the strain energy and maximum load-bearing capacity in the G5 model. However, a decrease in the maximum displacement capacity was concurrently noted. This suggests

Table 2 Properties of the GFRP-reinforced beams

Model code	Width (mm)	Depth (mm)	Tensile reinf. (ρ)	Comp. reinf. (ρ')	ρ-ρ'	Max. displ. (mm)	Max. load (kN)	Strain energy (kNm)	Failure mode*
G22	250	600	4ϕ12	2ϕ8	0.00245	160.55	148.20	13.48	G-R
G15	250	600	3ϕ14	2ϕ8	0.00251	159.77	150.80	13.72	G-R
G29	300	600	3ϕ16	2ϕ8	0.00291	156.16	163.80	14.43	G-R
G8	250	500	4ϕ12	2ϕ8	0.00296	190.49	99.00	10.62	G-R
G34	300	600	4ϕ14	2ϕ8	0.00299	165.34	172.90	16.14	G-R
G1	250	500	3ϕ14	2ϕ8	0.00304	194.70	102.30	11.20	G-R
G16	250	600	3ϕ16	2ϕ8	0.00350	166.11	192.40	17.71	G-R
G23	250	600	4ϕ14	2ϕ8	0.00358	166.41	195.00	17.88	G-R
G30	300	600	3ϕ18	2ϕ8	0.00384	161.98	202.80	18.18	G-R
G35	300	600	4ϕ16	2ϕ8	0.00408	170.33	218.40	20.49	G-R
G2	250	500	3ϕ16	2ϕ8	0.00423	190.70	123.75	13.00	G-R
G9	250	500	4ϕ14	2ϕ8	0.00434	206.65	135.30	15.28	G-R
G17	250	600	3ϕ18	2ϕ8	0.00461	173.49	239.20	22.61	G-R
G31	300	600	3ϕ20	2ϕ8	0.00488	191.05	273.00	28.60	G-R
G24	250	600	4ϕ16	2ϕ8	0.00490	174.00	249.60	23.63	G-R
G36	300	600	4ϕ18	2ϕ8	0.00532	178.59	273.00	26.55	G-R
G3	250	500	3ϕ18	2ϕ8	0.00558	216.00	165.00	19.95	C-C
G18	250	600	3ϕ20	2ϕ8	0.00586	177.00	296.40	29.81	G-R
G10	250	500	4ϕ16	2ϕ8	0.00593	214.20	171.60	19.91	C-C
G32	300	600	3ϕ22	2ϕ8	0.00603	181.74	300.30	29.77	C-C
G25	250	600	4ϕ18	2ϕ8	0.00638	173.23	296.40	27.93	C-C
G37	300	600	4ϕ20	2ϕ8	0.00670	174.87	313.95	30.84	C-C
G4	250	500	3ϕ20	2ϕ8	0.00709	198.48	180.40	19.43	C-C
G19	250	600	3ϕ22	2ϕ8	0.00723	166.95	312.00	28.33	C-C
G33	300	600	3ϕ24	2ϕ8	0.00728	169.61	323.70	29.88	C-C
G11	250	500	4ϕ18	2ϕ8	0.00772	192.84	188.10	19.60	C-C
G26	250	600	4ϕ20	2ϕ8	0.00804	156.71	319.80	27.19	C-C
G38	300	600	4ϕ22	2ϕ8	0.00823	160.77	336.70	29.45	C-C
G20	250	600	3ϕ24	2ϕ8	0.00874	153.87	332.80	27.83	C-C
G5	250	500	3ϕ22	2ϕ8	0.00876	176.71	189.20	18.09	C-C
G12	250	500	4ϕ20	2ϕ8	0.00974	176.54	204.60	19.52	C-C
G27	250	600	4ϕ22	2ϕ8	0.00988	139.95	335.40	25.45	C-C
G39	300	600	4ϕ24	2ϕ8	0.00991	151.20	364.00	29.91	C-C
G21	250	600	3ϕ26	2ϕ8	0.01038	143.30	353.60	27.48	C-C
G6	250	500	3ϕ24	2ϕ8	0.01058	170.33	209.00	17.95	C-C
G40	300	600	4ϕ26	2ϕ8	0.01173	139.04	382.20	28.89	C-C
G28	250	600	4ϕ24	2ϕ8	0.01189	136.77	373.10	27.76	C-C
G13	250	500	4ϕ22	2ϕ8	0.01196	163.18	220.30	19.44	C-C
G7	250	500	3ϕ26	2ϕ8	0.01257	157.61	220.00	17.91	C-C
G14	250	500	4ϕ24	2ϕ8	0.01439	150.81	234.30	19.15	C-C

* C-C: Crushing of concrete; G-R: Rupture of GFRP.

that while higher tensile reinforcement ratios enhance the load-bearing capacity, they may not necessarily improve the overall beam behavior. As detailed in Table 2, the failure mode transitioned from G-R for G2 to C-C for G5. While this shift resembles the transition from ductile to brittle fracture observed in steel-reinforced concrete

sections, it is crucial to note that the behavioral characteristics do not precisely mirror those of steel-reinforced concrete. Variations in the material properties, reinforcement ratios, and structural response underscore the distinctive nature of the observed transition in the G2 to G5 models.

While the reinforcement layouts of beams G7 and G13 differ, their other characteristics are nearly identical. Observations indicate that, despite the displacement capacity and strain energy of the G13 beam being 3.5% and 8.5% greater than those of the G7 beam, respectively, the load capacity remained consistent. This suggests that opting for a greater quantity of small-diameter reinforcement, as opposed to a lower quantity of large-diameter reinforcement, in GFRP-reinforced beams can positively influence the final displacement.

The sole distinction between the G4 and G19 beams lies in their section depths. The G4 beam, characterized by a lower section depth, exhibited an approximately 18.9% lower displacement capacity. Conversely, the G19 beam, with a greater section depth, demonstrates approximately 73% greater load-carrying capacity and 46% greater strain energy than does the G4 beam. This outcome highlights that, similar to that of steel-reinforced sections, the depth of the section has a more significant impact on the bearing capacity of GFRP-reinforced sections. Similarly, when comparing beams with different section widths and other features at the same level, it becomes evident that the influence of section width closely parallels the effect observed with section depth.

The CP (collapse prevention) limit for steel rebar in beams was set at 40% of the ultimate strain, in accordance with BECT-2018 [33]. Table 1 displays the maximum values of displacement, load, and strain energy for the CP limit state. The variation in the strain energy with respect to the cross-sectional area ($\sum E/A$) ratio with respect to the reinforcement ratio in the GFRP-reinforced beams is shown in Fig. 9. The average $\sum E/A$ limit value (125.4 kNm/m^2) of the steel-reinforced beams is also shown in Fig. 9. In addition, in Fig. 9, both the minimum reinforcement ratio limit recommended by ACI 440.1R-15 [10] and the minimum reinforcement ratio limit recommended by Eq. (20) in this study are shown. Accordingly, the recommended limit in this study is 70% greater than the limit recommended by ACI 440.1R-15 [10]. The minimum reinforcement ratio in GFRP-reinforced beams should be approximately 0.53% (Fig. 9). Therefore, Eq. (21) is proposed for a design that ensures that the energy of GFRP-reinforced beams is above the average energy of beams with steel rebar. According to this recommendation, considering the energy, the minimum reinforcement ratio should increase by 70% compared to the lower limit of the reinforcement ratio recommended by ACI 440.1R-15 [10].

$$\rho_f = 0.41\frac{\sqrt{f_c}}{f_{fu}} \geq \frac{2.3}{f_{fu}} \tag{20}$$

$$\rho_f = 0.70\frac{\sqrt{f_c}}{f_{fu}} \geq \frac{2.3}{f_{fu}} \tag{21}$$

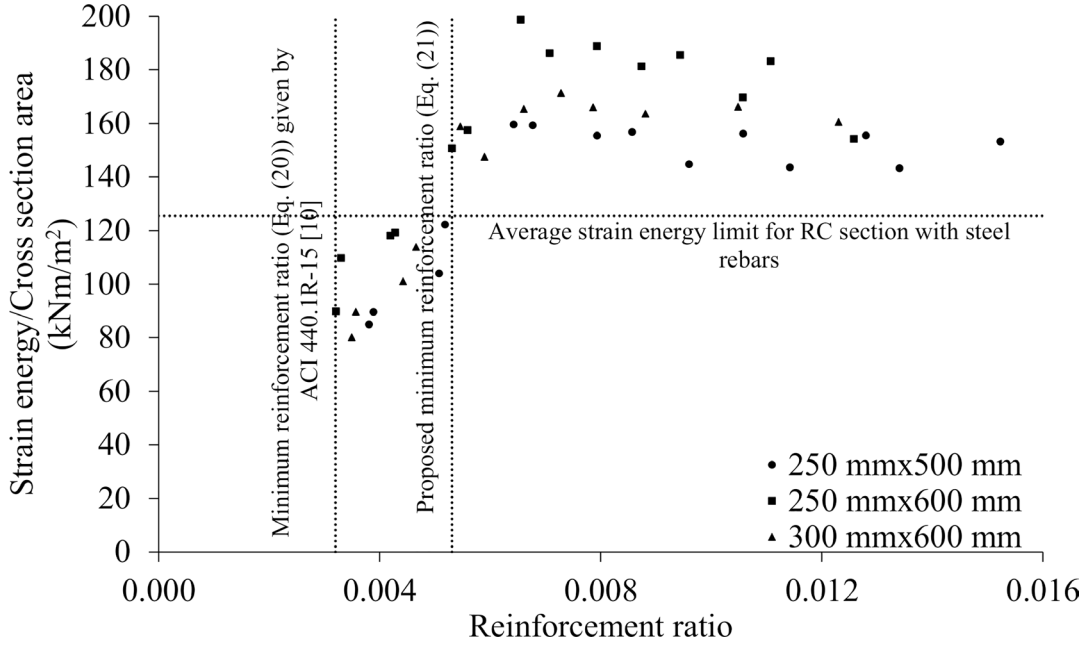

Fig. 9 Comparison of the strain energy versus the cross-sectional area ($\sum E/A$) rotil with respect to the reinforcement ratio in GFRP-reinforced beams

where ρ_f is the ratio of the reinforcement strength, f_c is the compressive strength of the concrete and f_{fu} is the tensile strength of the FRP rebar.

Depending on the tensile reinforcement ratio, beams with steel rebar can exhibit ductile or brittle behavior. If the steel rebar placed in the tensile zone yields before the concrete in the compression zone reaches its ultimate strain, the section will exhibit ductile behavior with tensile failure. However, the behavior of GFRP-reinforced beams is always brittle. This is because the GFRP rebar does not behave as ductile as the steel rebar when subjected to a tensile force. The behavior of GFRP-reinforced beams is always brittle, as fracture occurs through rupture of the GFRP rebar or crushing of the concrete. On the other hand, although brittle, GFRP-reinforced beams can dissipate as much energy as steel rebar beams. In other words, GFRP-reinforced beams can exhibit the desired behavior in terms of energy by disipating as much energy as ductile steel-reinforced sections if certain conditions are met. For this, it is clear that beams that provide the minimum reinforcement ratio in Eq. (19) will be safe. In addition, the results show that even if RC with GFRP rebar collapses when the concrete is crushed in the compression zone, the energy absorption capacity of these beams is greater than that corresponding to the collapse prevention (CP) performance limit of steel-reinforced beams.

The strain limit corresponding to the collapse prevention performance was determined for GFRP-reinforced beams that reached failure by crushing the concrete. These strain values are normalized with an alpha (α) coefficient defined in Eq. (22).

$$\alpha = \frac{\varepsilon_{CP}}{\varepsilon_{fu}} \tag{22}$$

where ε_{CP} is the strain in the GFRP rebar corresponding to collapse prevention and ε_{fu} (0.01934) is the ultimate strain in the GFRP rebar.

The change in the α coefficient with respect to the reinforcement ratio is shown in Fig. 10. Fig. 10 shows the variation in the α coefficient according to the reinforcement ratio, and a regression analysis was performed. Equation (23), which gives an α coefficient with an accuracy of 91.7%, was obtained. Here, ρ_f (%) shows the GFRP tensile reinforcement ratio. Equation (24) can be written to calculate the limit strain value for the CP. The CP strain values from the FEM were also calculated and are presented in Table 3. The highest absolute error rate among the results for both methods was found for the G24 beam (7.75%). This ratio is lower in the other models. This result shows that Eq. (24) can be used with a relatively small error rate.

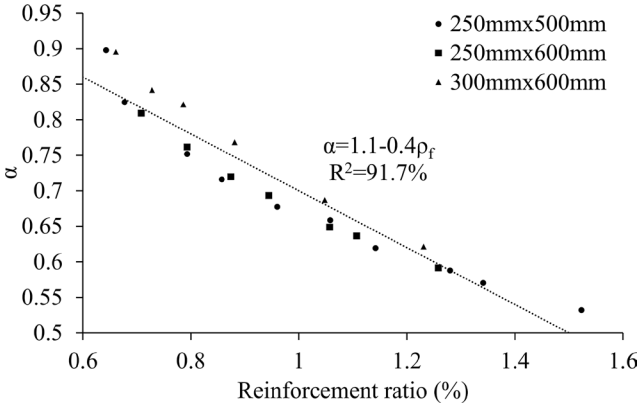

Fig. 10 Moment-curvature relationships of steel and FRP-reinforced beams for the design moment

Table 3 Comparison of strain values corresponding to CP

Model code	Strain corr. to CP		Abs. err. (%)
	FEM	Eq. (24)	
G3	0.0174	0.0163	6.16
G4	0.0145	0.0151	4.12
G5	0.0131	0.0138	5.71
G6	0.0120	0.0124	3.84
G7	0.0110	0.0109	1.18
G10	0.0160	0.0160	0.54
G11	0.0139	0.0146	5.73
G12	0.0127	0.0131	2.74
G13	0.0114	0.0114	0.02
G14	0.0103	0.0095	7.75
G19	0.0147	0.0151	2.78
G20	0.0134	0.0140	4.19
G21	0.0123	0.0127	3.25
G25	0.0157	0.0158	0.94
G26	0.0139	0.0145	4.26
G27	0.0126	0.0131	4.36
G28	0.0114	0.0115	0.89
G32	0.0173	0.0162	6.69
G33	0.0159	0.0152	4.38
G37	0.0163	0.0156	3.92
G38	0.0149	0.0145	2.70
G39	0.0133	0.0132	0.93
G40	0.0120	0.0118	2.24

In the classical RC design process, the yield point of the steel is taken as a basis point in the sectional design. The behaviors of the GFRP rebar and conventional steel rebar are different from each other under tensile forces.

Since GFRP rebar subjected to tensile forces exhibit approximately linear elastic behavior until fracture, the ultimate strain or strength of the GFRP rebar should be reduced when designing GFRP-reinforced beams. Hence, RC beams incorporating GFRP rebar can be engineered to ensure compliance with the CP limit. The CP limit strain of the GFRP rebar necessary for the design of such RC beams can be determined using Eq. (23). Additionally, the α coefficient outlined in Eq. (23) can be considered a potential reduction factor for the strength of the GFRP rebar owing to its linear elastic behavior.

$$\alpha = 1.1 - 0.4\rho_f \tag{23}$$

$$\varepsilon_{\mathrm{CP}} = \alpha\varepsilon_{fu} \tag{24}$$

5.2 Crack propagation in beams

In Fig. 11, the crack patterns of both the steel and GFRP-reinforced concrete beams reaching their final state through concrete crushing are depicted. The crack pattern assessment was conducted across four distinct load levels, ranging from 0.25P to 1.00P (final state), representing a progression from low to high loads. The evaluation reveals an increase in the crack density with increasing load for both types of reinforcement. Notably, in the GFRP-reinforced beams, the cracks are closer to the support area and more intense, particularly at the 0.75P and 1.0P levels. Notably, while tensile cracks do not manifest in steel-reinforced beams at 25% of the ultimate load (0.25P), GFRP-reinforced beams exhibit tensile cracks at this load level. The reason is that the initial stiffness of the steel rebar is greater than that of the GFRP rebar. Differences have been observed in the development of tensile cracks in steel-reinforced and GFRP-reinforced beams. Tensile cracks in steel-reinforced beams rapidly increase in the later stages of loading, usually after the steel rebar yield. In GFRP-reinforced beams, because the GFRP rebar will not yield, such a sudden increase does not occur. Instead, an increasing crack width can be observed in proportion to the Table 4. Comparison of strain values corresponding to CP magnitude of the tensile force due to possible weak bond strengths between the GFRP rebar and the concrete. The bond strength is relevant to the concrete strength and surface shape of the GFRP rebar. As the concrete strength increases, the bond strength increases. In addition, after the first crack is formed in both beams, the cracks progress toward the support zone. As a general result, it has been determined that beams with GFRP rebar have greater crack density than RC beams with steel rebar. Adam et al. [14] experimentally and analytically investigated crack patterns in GFRP-reinforced beams. The crack patterns observed in this study and their results are similar.

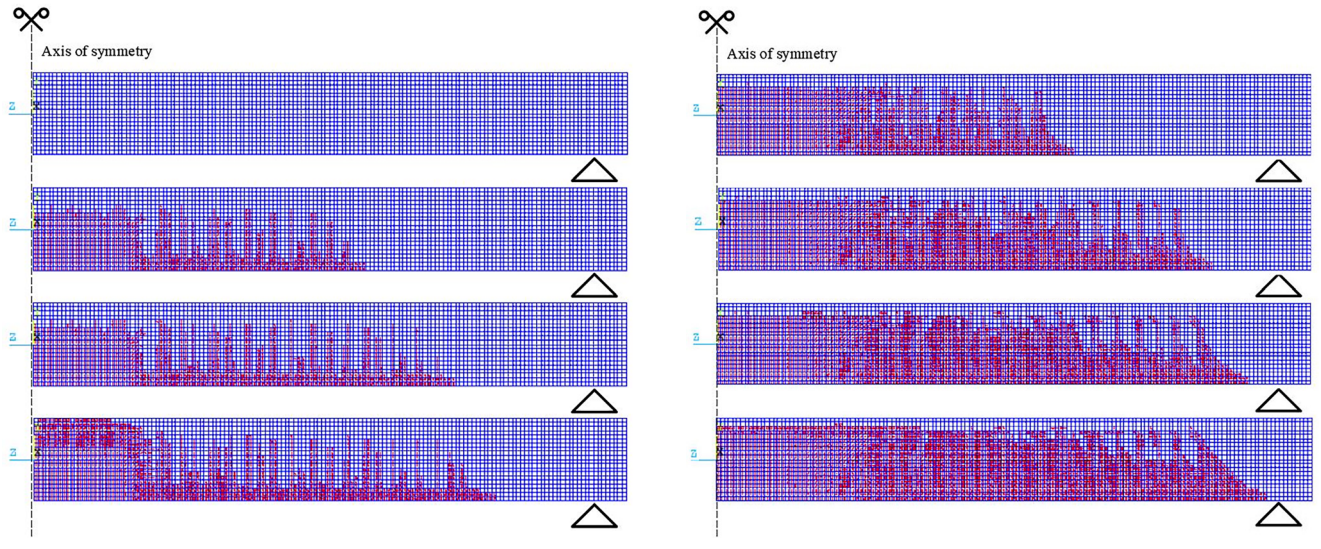

(a) (b)

Fig. 11 Crack propagation for different load steps in RC beams: (a) RC beam with steel rebars (b) RC beam with GFRP rebars

Table 4 Performance of different equations according to χ

	Eq. (1)	Eq. (2)	Eq. (3)	Eq. (4)	Eq. (5)	Eq. (6)	Eq. (7)	Proposed Eq.
χ	1.22	1.21	1.18	1.23	1.20	1.43	1.18	1.17

5.3 Investigation of the section stiffness of RC beams with GFRP rebars

Regardless of the type of reinforcement used, RC elements are inherently composite structures. Given the inherently low tensile strength of concrete, tensile cracks can form in RC members even under relatively low external loads. These cracks alter the moments of inertia of the section, consequently affecting the flexural stiffness. As a result, significant variations in the internal forces arise. Hence, the precision of internal force calculations is contingent upon accurately determining the cracked section stiffness of the designed elements. In this section, we propose the use of GFRP-reinforced beams by comparing the cracked/uncracked section stiffnesses obtained from the finite element models and from the effective moments of inertia suggested in the literature. In this context, the cracked and uncracked section stiffnesses of the finite element models were calculated. The load–displacement relationship of the GFRP-reinforced beams was used in the calculation of these stiffnesses. The load–displacement relationship of the GFRP-reinforced beams is approximately bilinear. The slope of the first linear part in the load–displacement relationship gives the uncracked section stiffness, while the slope of the second linear part gives the cracked section stiffness. In the present study, the cracked/uncracked section stiffnesses were obtained by proportioning these stiffnesses obtained from finite element models.

The cracked/uncracked section stiffness ratios were determined by using well-known equations from the literature and common regulations, and they are given in Fig. 12. Fig. 12 also shows the cracked/uncracked section stiffness ratios, which are calculated from FEM analysis and from the proposed equation. The effective moment of inertia can be calculated accurately using the equation transformed by these coefficients [9, 10, 19–23].

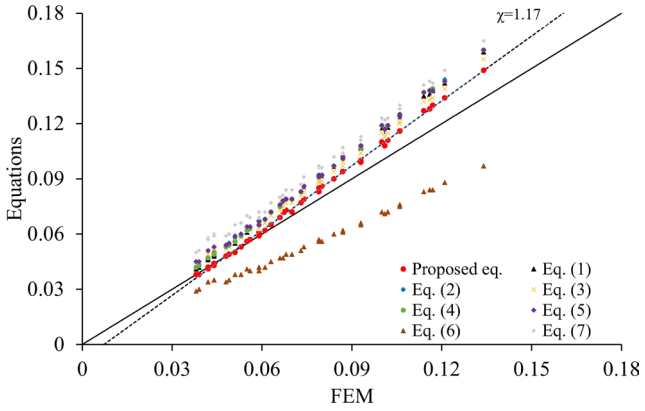

Fig. 12 Comparison of the ratio of cracked stiffness to uncracked stiffness using different methods

The effective moment of inertia recommended in TS 500 [46] and ACI 318-14 [48] for conventional RC elements has been revised using the coefficient β_d from ACI 440.1R-06 [9] for use in FRP reinforced elements (Eq. (2)). Alongside this coefficient, Habeeb and Ashour [23] proposed the inclusion of the γ_G coefficient (Eq. (6)) in the equations, while Rafi and Nadjai [20] recommended incorporating the γ coefficient (Eq. (3)) into the formulas. However, these coefficients still need to be improved. In this context, instead of the coefficients suggested by ACI 440.1R-06 [9], Habeeb and Ashour [23]; and Rafi and Nadjai [20], the coefficients $\beta_d = 0.05$ and $\gamma_G = 0.95$, which are more compatible with the FEM models, are proposed. These proposed coefficients show the best fit with FEM models as a result of various iterations. The coefficient of determination (R^2) between the results obtained using $\beta_d = 0.05$ and $\gamma_G = 0.95$ and the FEMs was determined to be 99.92%. This situation reveals that the effective moment of inertia works quite well with the use of these coefficients.

The cracked/uncracked section stiffnesses were calculated using different methods for the RC beams with GFRP rebar (Fig. 12). This ratio was determined to be 0.055 for the G2 beam, whose FEM was created. These values were found to be 10.9%, 16.4%, 12.7%, 12.7%, 16.4% and 27.2% higher in ACI 440.1R-06 [9]; ACI 440.1R-15 [10]; Bischoff [19, 22]; Rafi and Nadjai [20]; and ISIS [21], respectively. However, this value is calculated to be 25.4% less when the equation suggested by Habeeb and Ashour [23] is used. This difference was found to be 1.8% greater when calculated with the proposed equation. For a clearer understanding of the variation, χ is examined in Fig. 12. This variable serves as a general performance indicator, representing the slope of the line obtained from the linear regression analysis. According to this indicator, the model that demonstrates the best performance is the equation proposed with a value of 1.17 (Fig. 12). The performance of the other equations is lower than that of the proposed equation, as shown in Table 4. Therefore, more accurate results can be obtained when using Eq. (25).

$$I_e = 0.05\left(\frac{M_{cr}}{M_a}\right)^3 I_g + 0.95\left[1-\left(\frac{M_{cr}}{M_a}\right)^3\right] I_{cr} \le I_g \qquad (25)$$

Sensitivity analysis for Eq. (25) was conducted using the Sobol sensitivity index [49]. The input parameter boundaries were evaluated with 1000 samples, utilizing the Latin Hypercube Sampling (LHS) method [50]. Subsequently, the Sobol sensitivity index was calculated through 1000 bootstrap repetitions (Table 5). The parameter M_a, with a value of 0.701, was identified as the most

Table 5 Sobol indices results

Parameters	Sobol indices	bias	std. error	min. c. i.	max. c. i.
Mcr	0.188	0.013	0.080	−0.014	0.291
Ma	0.701	0.020	0.172	0.288	0.963
Ig	0.069	0.006	0.049	−0.057	0.144
Icr	0.064	0.006	0.048	−0.057	0.138

min. c. i.: Minimum confidence interval
max. c. i.: Maximum confidence interval

sensitive. Meanwhile, the sensitivities of I_g and I_{cr} were the closest to each other and exhibited the lowest sensitivity.

6 Conclusions

Suggestions for modifications to certain equations concerning RC beams with GFRP rebar were provided. The following conclusions can be drawn from the results of this study:

- While the strain energy increases with increasing reinforcement ratio in under-reinforced beams, it remains relatively constant in over-reinforced beams, even as the reinforcement ratio may increase. Consequently, maintaining the reinforcement ratio close to the balanced level yields optimal results for strain energy. According to the results of this study, Eq. (21) is suggested instead of Eq. (20) so that GFRP-reinforced beams can meet the strain energy provided by steel-reinforced beams.
- For the collapse prevention limit, the strain of the GFRP rebar can be calculated by Eq. (24), which is based on the tensile reinforcement ratio.
- It is recommended that the effective moment of inertia equation for GFRP-reinforced concrete elements be revised with coefficients of 0.05 and 0.95, as presented in Eq. (25). These revisions significantly improved the overall performance indicator, increasing it to 1.17.
- Despite maintaining a consistent load capacity, the beam with a 3.5% higher displacement capacity and 8.5% greater strain energy benefitted from a higher quantity of small-diameter rebar. This finding indicates that increasing the amount of small-diameter reinforcement in GFRP-reinforced beams can enhance displacement performance without affecting load-bearing capacity.
- Increasing the section depth by 20% results in approximately 73% higher load-carrying capacity and 46% greater strain energy. The shallower section shows an 18.9% lower displacement capacity.
- While the crack patterns of the GFRP-reinforced beams generally resemble those of the steel-reinforced beams, notable differences were observed. Specifically, cracks in GFRP-reinforced beams tended to be more intense and widespread across the beam span, particularly at service load levels.

7 Recommendations

The current study opens several avenues for future research and analysis:

- While the flexural behavior has been investigated through numerical models and equations have been proposed based on these models, future research could involve extensive experimental testing to validate the performance of these proposed equations.
- Comprehensive cost-benefit analyses could be conducted to evaluate the impact of section depth on load-carrying capacity and strain energy, providing a more detailed understanding of economic and performance considerations.
- The analyses in this study are limited to GFRP rebars. Future research could extend these studies to other types of reinforcement, such as CFRP (Carbon Fiber Reinforced Polymer), AFRP (Aramid Fiber Reinforced Polymer), and BFRP (Basalt Fiber Reinforced Polymer), to compare their performance and applicability.
- The investigation of flexural behavior has been restricted to rectangular cross-section reinforced concrete beams. Future studies could explore the effects of different cross-sectional shapes, such as slab-type cross-sections, on beam flexural behavior.

References

[1] Yuksel, I., Sakcalı, G. B. "Effects of reinforcement corrosion on reinforced concrete buildings", Proceedings of the Institution of Civil Engineers: Structures and Buildings, 175(3), pp. 244–258, 2022. https://doi.org/10.1680/JSTBU.19.00111

[2] Shayanfar, M. A., Barkhordari, M. A., Ghanooni-Bagha, M. "Estimation of Corrosion Occurrence in RC Structure Using Reliability Based PSO Optimization", Periodica Polytechnica Civil Engineering, 59(4), pp. 531–542, 2015. https://doi.org/10.3311/PPCI.7588

[3] Ghanooni-Bagha, M., Zarei, S., Savoj, H. R., Shayanfar, M. A. "Time-dependent Seismic Performance Assessment of Corroded Reinforced Concrete Frames", Periodica Polytechnica Civil Engineering, 63(2), pp. 631–640, 2019. https://doi.org/10.3311/PPCI.12653

[4] Stoner, J. G., Polak, M. A. "Finite element modelling of GFRP reinforced concrete beams", Computers and Concrete, 25(4), pp. 369–382, 2020. https://doi.org/10.12989/CAC.2020.25.4.369

[5] Anand, N., Kiran, T., Lubloy, E., Mathews, M. E., Kanagaraj, B., Andrushia, D. "Flexural Behavior of Reinforced Concrete Beams with FRP Bars Exposed to Elevated Temperature", Periodica Polytechnica Civil Engineering, 67(1), pp. 93–101, 2023. https://doi.org/10.3311/PPCI.20950

[6] Kaya, N., Avanoğlu Sicacik, E., Bakirci Er, Ş., Kopraman, Y., Büyükkaragöz, A. "The effects of reinforcement ratio on flexural behavior in hybrid (GFRP-Steel) reinforced concrete beams", Journal of Polytechnic, 24(3), pp. 1109–1119, 2021. https://doi.org/10.2339/POLITEKNIK.817398

[7] Sakcalı, G. B., Yüksel, İ. "Shear Strength Evaluation of Concrete Beams with FRP Transverse Rebar", Periodica Polytechnica Civil Engineering, 68(2), pp. 469–485, 2024. https://doi.org/10.3311/PPci.22324

[8] Sakcalı, G. B., Yüksel, İ., Sağıroğlu, S. "Experimental investigation of flexural bond behavior of sand-coated GFRP rebar embedded in concrete", Journal of Building Engineering, 87, 109113, 2024. https://doi.org/10.1016/J.JOBE.2024.109113

[9] ACI Committee 440 "ACI 440.1R-06: Guide for the design and construction of structural concrete reinforced with FRP bars", American Concrete Institute, Farmington Hills, MI, USA, 2006.

[10] ACI Committee 440 "ACI 440.1R-15: Guide for the Design and Construction of Structural Concrete Reinforced with Fiber-Reinforced Polymer (FRP) Bars", American Concrete Institute, Farmington Hills, MI, USA, 2015.

[11] Canadian Standards Association "CSA S6-14: Canadian highway bridge design code", CSA Group, Toronto, Canada, 2014.

[12] Canadian Standards Association "CSA S806-12 (R2021): Design and construction of building components with fibre reinforced polymers", CSA Group, Toronto, Canada, 2012.

[13] Kara, I. F., Ashour, A. F. "Flexural performance of FRP reinforced concrete beams", Composite Structures, 94(5), pp. 1616–1625, 2012. https://doi.org/10.1016/j.compstruct.2011.12.012

[14] Adam, M. A., Said, M., Mahmoud, A. A., Shanour, A. S. "Analytical and experimental flexural behavior of concrete beams reinforced with glass fiber reinforced polymers bars", Construction and Building Materials, 84, pp. 354–366, 2015. https://doi.org/10.1016/j.conbuildmat.2015.03.057

[15] Sirimontree, S., Keawsawasvong, S., Thongchom, C. "Flexural behavior of concrete beam reinforced with GFRP bars compared to concrete beam reinforced with conventional steel reinforcements", Journal of Applied Science and Engineering, 24(6), pp. 883–890, 2021. https://doi.org/10.6180/jase.202112_24(6).0009

[16] Sasikumar, P., Manju, R. "Flexural behaviour of reinforced concrete beams reinforced with Glass Fibre Reinforced Polymer (GFRP) bars: experimental and analytical study", Asian Journal of Civil Engineering, 25(4), pp. 3623–3636, 2024. https://doi.org/10.1007/s42107-024-01000-4

[17] Kinjawadekar, T. A., Patil, S., Nayak, G. "A Critical Review on Glass Fiber-Reinforced Polymer Bars as Reinforcement in Flexural Members", Journal of The Institution of Engineers (India): Series A, 104(2), pp. 501–516, 2023. https://doi.org/10.1007/s40030-023-00729-6

[18] Vijay, P. V., GangaRao, H. V. S. "Bending behavior and deformability of glass fiber-reinforced polymer reinforced concrete members", ACI Structural Journal, 98(6), pp. 834–842, 2001. https://doi.org/10.14359/10750

[19] Bischoff, P. H. "Reevaluation of deflection prediction for concrete beams reinforced with steel and fiber reinforced polymer bars", Journal of Structural Engineering, 131(5), pp. 752–767, 2005. https://doi.org/10.1061/(ASCE)0733-9445(2005)131:5(752)

[20] Rafi, M. M., Nadjai, A. "Evaluation of ACI 440 Deflection Model for Fiber-Reinforced Polymer Reinforced Concrete Beams and Suggested Modification", ACI Structural Journal, 106(6), pp. 762–771, 2009. https://doi.org/10.14359/51663177

[21] Newhook, J., Svecova, D. "Reinforcing concrete structures with fibre reinforced polymers", ISIS Canada Research Network, Design manual No. 3, Version 2, 2007. ISBN 0-9689006-6-6

[22] Bischoff, P. H. "Deflection calculation of FRP reinforced concrete beams based on modifications to the existing Branson equation", Journal of Composites for Construction, 11(1), pp. 4–14, 2007. https://doi.org/10.1061/(ASCE)1090-0268(2007)11:1(4)

[23] Habeeb, M. N., Ashour, A. F. "Flexural Behavior of Continuous GFRP Reinforced Concrete Beams", Journal of Composites for Construction, 12(2), pp. 115–124, 2008. https://doi.org/10.1061/(ASCE)1090-0268(2008)12:2(115)

[24] Zhu, C., Sun, L., Wang, K., Yuan, Y., Wei, M. "Effect of bond slip on the performance of FRP reinforced concrete columns under eccentric loading", Computers and Concrete, 24(1), pp. 73–83, 2019. https://doi.org/10.12989/cac.2019.24.1.073

[25] Jumaa, G. B., Yousif, A. R., "Numerical modeling of size effect in shear strength of FRP-reinforced concrete beams", Structures, 20, pp. 237–254, 2019. https://doi.org/10.1016/j.istruc.2019.04.008

[26] Sakcalı, G. B., Yüksel, İ., Sağıroğlu, S. "Experimental and numerical investigation of the bond behavior of smooth and sand-coated rebar in concrete by flexural bond test method", Journal of Polytechnic, 27(2), pp. 709–720, 2024. https://doi.org/10.2339/POLITEKNIK.1097459

[27] ASTM International "ASTM D7205/D7205M-06(2011): Standard test method for tensile properties of fiber reinforced polymer matrix composite bars", ASTM International, West Conshohocken, PA, USA, 2011. https://doi.org/10.1520/D7205_D7205M-06R11

[28] ACI Committee 440 "ACI PRC-440-07: Report on fiber-reinforced polymer (FRP) reinforcement for concrete structures", American Concrete Institute, Farmington Hills, MI, USA, 2007.

[29] Swanson Analysis System, Inc. "ANSYS simulation software (Version 15)", [computer program] Swanson Analysis System, Inc., Canonsburg, PA, USA, 2013.

[30] Subramani, T., Manivannan, R., Kavitha, M. "Crack Identification in Reinforced Concrete Beams Using Ansys Software", International Journal of Engineering Research and Applications, 4(6), pp. 133–141, 2014.

[31] Bangash M. Y. H. "Concrete and concrete structures: Numerical modelling and applications", Elsevier Applied Science, 1989. ISBN 1-85166-294-4

[32] Kachlakev, D., Miller, T. R., Yim, S., Chansawat, K., Potisuk, T. "Finite element modeling of concrete structures strengthened with FRP laminates", Oregon Department of Transportation Research Group, Federal Highway Administration, Rep. FHWA-OR-RD-01-17, 2001.

[33] Ministry Regulation Committee "Deprem Etkisi Altındaki Binaların Tasarım İlkeleri" (BECT-2018: Building Earthquake Code of Turkey), [pdf] Ministry of Interior of the Republic of Turkey, Ankara, Turkey, 2018. Available at: https://www.resmigazete.gov.tr/eskiler/2018/03/20180318M1-2-1.pdf (in Turkish)

[34] Ersoy U., Özcebe G., Tankut, T. "Reinforced concrete", Middle East Technical University (METU), Ankara, Turkey, 2006.

[35] Willam, K. J., Warnke, E. P. "Constitutive model for the triaxial behavior of concrete", In: International Association for Bridge and Structural Engineering, Bergamo, Italy, vol. 19, 1974, III-1. ISBN 3 85748 007 6

[36] Wolanski, A. J. "Flexural behavior of reinforced and prestressed concrete beams using finite element analysis", MSc Thesis, Marquette University, 2004.

[37] El-Mogy, M., El-Ragaby, A., El-Salakawy, E. "Behaviour of Continuous Concrete Beams Reinforced with FRP Bars", In: Ye, L., Feng, P., Yue, Q. (eds.) Advances in FRP Composites in Civil Engineering, Springer, 2011, pp. 283–286. ISBN 978-3-642-17486-5 https://doi.org/10.1007/978-3-642-17487-2_60

[38] fib Special Activity Group 5 "Model Code 2010 - First complete draft, Volume 1", International Federation for Structural Concrete (fib), fib Bulletin No. 55, 2010. ISBN 978-2-88394-095-6 https://doi.org/10.35789/fib.BULL.0055

[39] Vint, L. M. "Investigation of bond properties of glass fibre reinforced polymer (GFRP) bars in concrete under direct tension", MSc Thesis, University of Toronto, 2012.

[40] Kato, J. "Material Optimization for Fiber Reinforced Composites applying a Damage Formulation", Doctor of Engineering Dissertation, Universität Stuttgart, 2010. ISBN 978-3-00-030186-5

[41] Murthy, A. R., Palani, G. S., Iyer, N. R., Gopinath, S., Kumar, V. R. "Impact failure analysis of reinforced concrete structural components by using finite element method", Computer Modeling in Engineering & Sciences, 86(5), pp. 409–434, 2012. https://doi.org/10.3970/cmes.2012.086.409

[42] Azimi, M., Ponraj, M., Bagherpourhamedani, A., Tahir, M. M., Razak, S. M. S. A., Pheng, O. P. "Shear capacity evaluation of reinforced concrete beams: Finite element simulation", Jurnal Teknologi, 77(16), pp. 59–66, 2015. https://doi.org/10.11113/jt.v77.6400

[43] Tavárez, F. A. "Simulation of Behavior of Composite Grid Reinforced Concrete Beams Using Explicit Finite Element Methods", MSc Thesis, University of Wisconsin-Madison, 2001.

[44] Barris, C., Torres, L. I., Turon, A., Baena, M., Catalan, A. "An experimental study of the flexural behaviour of GFRP RC beams and comparison with prediction models", Composite Structures, 91(3), pp. 286–295, 2009. https://doi.org/10.1016/j.compstruct.2009.05.005

[45] Ovitigala, T., Ibrahim, M. A., Issa, M. A. "Serviceability and ultimate load behavior of concrete beams reinforced with basalt fiber-reinforced polymer bars", ACI Structural Journal, 113(4), pp. 757–768, 2016. https://doi.org/10.14359/51688752

[46] Turkish Standards Institute "TS 500: Requirements for design and construction of reinforced concrete structures", Turkish Standards Institute, Ankara, Turkey, 2000.

[47] Ifrahim, M. S., Sangi, A. J., Ahmad, S. H. "Experimental and numerical investigation of flexural behaviour of concrete beams reinforced with GFRP bars", Structures, 56, 104951, 2023. https://doi.org/10.1016/j.istruc.2023.104951

[48] ACI Committee 318 "Building code requirements for structural concrete (ACI 318-14) and commentary on building code requirements for structural concrete (ACI 318R-14)", American Concrete Institute, Farmington Hills, MI, USA, 2014.

[49] Saltelli, A., Sobol, I. M. "Sensitivity analysis for non-linear mathematical models: numerical experience", Mathematical Models and Computer Experiment, 7(11), pp. 16–28, 1995. (in Russian)

[50] McKay, M. D., Beckman, R. J., Conover, W. J. "A Comparison of Three Methods for Selecting Values of Input Variables in the Analysis of Output from a Computer Code", Technometrics, 21(2), pp. 239–245, 1979. https://doi.org/10.2307/1268522